A physically based model of global freshwater surface temperature

Ludovicus P. H. van Beek,[1] Tessa Eikelboom,[1,2] Michelle T. H. van Vliet,[3] and Marc F. P. Bierkens[1,4]

Received 4 January 2012; revised 15 May 2012; accepted 19 July 2012; published 20 September 2012.

[1] Temperature determines a range of physical properties of water and exerts a strong control on surface water biogeochemistry. Thus, in freshwater ecosystems the thermal regime directly affects the geographical distribution of aquatic species through their growth and metabolism and indirectly through their tolerance to parasites and diseases. Models used to predict surface water temperature range between physically based deterministic models and statistical approaches. Here we present the initial results of a physically based deterministic model of global freshwater surface temperature. The model adds a surface water energy balance to river discharge modeled by the global hydrological model PCR-GLOBWB. In addition to advection of energy from direct precipitation, runoff, and lateral exchange along the drainage network, energy is exchanged between the water body and the atmosphere by shortwave and longwave radiation and sensible and latent heat fluxes. Also included are ice formation and its effect on heat storage and river hydraulics. We use the coupled surface water and energy balance model to simulate global freshwater surface temperature at daily time steps with a spatial resolution of 0.5° on a regular grid for the period 1976–2000. We opt to parameterize the model with globally available data and apply it without calibration in order to preserve its physical basis with the outlook of evaluating the effects of atmospheric warming on freshwater surface temperature. We validate our simulation results with daily temperature data from rivers and lakes (U.S. Geological Survey (USGS), limited to the USA) and compare mean monthly temperatures with those recorded in the Global Environment Monitoring System (GEMS) data set. Results show that the model is able to capture the mean monthly surface temperature for the majority of the GEMS stations, while the interannual variability as derived from the USGS and NOAA data was captured reasonably well. Results are poorest for the Arctic rivers because the timing of ice breakup is predicted too late in the year due to the lack of including a mechanical breakup mechanism. Moreover, surface water temperatures for tropical rivers were overestimated, most likely due to an overestimation of rainfall temperature and incoming shortwave radiation. The spatiotemporal variation of water temperature reveals large temperature differences between water and atmosphere for the higher latitudes, while considerable lateral transport of heat can be observed for rivers crossing hydroclimatic zones, such as the Nile, the Mississippi, and the large rivers flowing to the Arctic. Overall, our model results show promise for future projection of global surface freshwater temperature under global change.

Citation: van Beek, L. P. H., T. Eikelboom, M. T. H. van Vliet, and M. F. P. Bierkens (2012), A physically based model of global freshwater surface temperature, *Water Resour. Res.*, *48*, W09530, doi:10.1029/2012WR011819.

1. Introduction

[2] Temperature directly determines a range of physical properties of surface water including vapor pressure, surface tension, density and viscosity, and the solubility of oxygen and other gases. Indirectly water temperature acts as a strong control on freshwater biogeochemistry, influencing sediment concentration and transport, water quality parameters (e.g., pH, nitrogen, phosphor, dissolved oxygen), chemical reaction rates, phytoplankton and zooplankton composition and the presence or absence of pathogens [*Webb*, 1996; *Rounds et al.*, 1999]. Thus, in freshwater ecosystems the thermal

[1]Department of Physical Geography, Utrecht University, Utrecht, Netherlands.
[2]Institute for Environmental Studies, Vrije Universiteit, Amsterdam, Netherlands.
[3]Earth System Science and Climate Change, Wageningen University and Research Centre, Wageningen, Netherlands.
[4]Unit Soil and Groundwater, Deltares, Utrecht, Netherlands.

Corresponding author: L. P. H. van Beek, Department of Physical Geography, Utrecht University, NL-3508 TC Utrecht, Netherlands. (r.vanbeek@uu.nl)

0043-1397/12/2012WR011819

regime affects the geographical distribution of aquatic species through their growth and metabolism, tolerance to parasites, diseases and pollution and life history in general [*Beitinger et al.*, 2000; *Burgmer et al.*, 2007].

[3] Past work on modeling freshwater surface temperature (see *Webb et al.* [2008] for an extensive review of methods) can be divided into statistical methods establishing regression-type relationships between water temperature and air temperature and stream discharge or flow velocity [*Neumann et al.*, 2003; *Donato*, 2003; *Benyahya et al.*, 2007] and physically based deterministic modeling of water flow and the water energy balance [*Wang and Martin*, 1991; *Kim and Chapra*, 1997; *Caissie et al.*, 2007]. Temperature models of lakes are among the most sophisticated of deterministic freshwater temperature models [*Perroud et al.*, 2009], including density effects and temperature stratification, turbulent vertical mixing and wind action (e.g., in order of increasing complexity: *Mironov* [2008]; *Goudsmit et al.* [2002]; *Hodges et al.* [2000]). When compared to statistical approaches, physically based deterministic models have the advantage that they are more robust to changes in flow regime, river morphology, radiation balance and upstream hydrology. Such models are therefore better suited for projecting the effects of global change on water temperature.

[4] Until now, physically based deterministic models have only been applied to well-defined freshwater bodies of limited size (e.g., lakes or stream segments), where the numerous parameters can be measured or otherwise established. However, in order to support global studies on the effect of the climate change and direct anthropogenic impacts on freshwater ecosystem health and biodiversity, e.g., as part of integrated assessments [cf. *Vörösmarty et al.*, 2010], global models of freshwater temperature dynamics are required. To this end, *van Vliet et al.* [2011] presented one of the first attempts to model global river water temperature using a nonlinear regression model of water temperature and discharge. Here, we present the initial results from a physically based deterministic model of global freshwater surface temperature. The model adds a surface water energy balance to river discharge modeled by the global hydrological model PCR-GLOBWB. In addition to advection of energy from direct precipitation, runoff and lateral exchange along the drainage network, energy is exchanged between the water body and the atmosphere by shortwave and longwave radiation and sensible and latent heat fluxes. Also included are ice formation and its effect on heat storage and river hydraulics. We used the coupled surface water and energy balance model to simulate global freshwater surface temperature at daily time steps with a spatial resolution of 0.5° on a regular grid for the period from 1976 to 2000 inclusive. We compared our simulation results with daily temperature data from rivers and lakes (U.S. Geological Survey (USGS), limited to the USA) and compared mean monthly temperatures with those recorded in the Global Environment Monitoring System (GEMS) data set.

[5] In the remaining part of the paper we first introduce the global hydrological model and the water energy balance module. Next follows a short description of the temperature data used and a description of the validation results. Thereafter, we investigate how surface water temperature differs from air temperature along river stretches and across climate zones. We end the paper with the discussion and conclusion.

2. Physically Based Model of Global Freshwater Temperature

2.1. Global Hydrological Model PCR-GLOBWB

[6] In order to properly model the energy balance of terrestrial freshwater resources, advection of water through rivers, lakes and reservoirs needs to be taken into account, as well as the generation of runoff, i.e., the conversion of precipitation into various runoff components, each with its own temperature signature. To model both runoff generation as well as freshwater advection we used the global hydrological model PCR-GLOBWB [*van Beek et al.*, 2011] (Figure 1). PCR-GLOBWB calculates for each grid cell (0.5° × 0.5° globally) and for each time step (daily) the water storage in two vertically stacked soil layers and an underlying groundwater layer, as well as the water exchange between the layers and between the top layer and the atmosphere (rainfall, evaporation and snowmelt). The model also calculates canopy interception and snow storage. Subgrid variability is taken into account by considering separately tall and short vegetation, open water, different soil types and the fractional area of saturated soil and the frequency distribution of groundwater depth based on the surface elevations of the 1 × 1 km Hydro1k data set [*Verdin and Greenlee*, 1996] (Land Processes Distributed Active Archive Center, HYDRO1k Elevation Derivative Database, http://eros.usgs.gov/#/Find_Data/Products_and_Data_Available/gtopo30/hydro). Fluxes between the lower soil reservoir and the groundwater reservoir are mostly downward, except for areas with shallow groundwater tables, where fluxes from the groundwater reservoir to the soil reservoirs are possible (i.e., capillary rise) during periods of low soil moisture content. The total specific runoff of a cell consists of saturation excess surface runoff, meltwater that does not infiltrate, runoff from the second soil reservoir (interflow) and groundwater runoff (base flow) from the lowest reservoir. To calculate river discharge, specific runoff is accumulated along the drainage network by means of kinematic wave routing [*Chow et al.*, 1988]. The kinematic wave approximation neglects the terms of the momentum equation other than slope in the Saint-Venant equations and is therefore less applicable for rivers with slight slopes that often exhibit hysteresis. Notwithstanding, the resulting errors are generally small and the velocity of the main part of natural flood waves approximates that of a kinematic wave [*Lighthill and Whitham*, 1955]. Included in the routing scheme are the storage effects and evaporative losses from lakes, reservoirs and wetlands. Required channel dimensions are obtained from established relationships between bankfull discharge and channel geometry and hydraulic properties from the literature (see *van Beek and Bierkens* [2009] for details and references). This routing scheme is explicit and subdaily time steps are used to preserve stability (variable time stepping based on the courant number), assuming uniform local input rates of energy and water during the day. Daily discharge is then reported as the average lateral flux through the cell while water height, water temperature and ice thickness are reported at the end of the day. For this study, PCR-GLOBWB was forced with 44 years (1958–2001) of daily fields of precipitation and temperature (at 2 m above surface level), which comply with the monthly values of the observation based CRU TS 2.1 at a spatial resolution of 0.5°

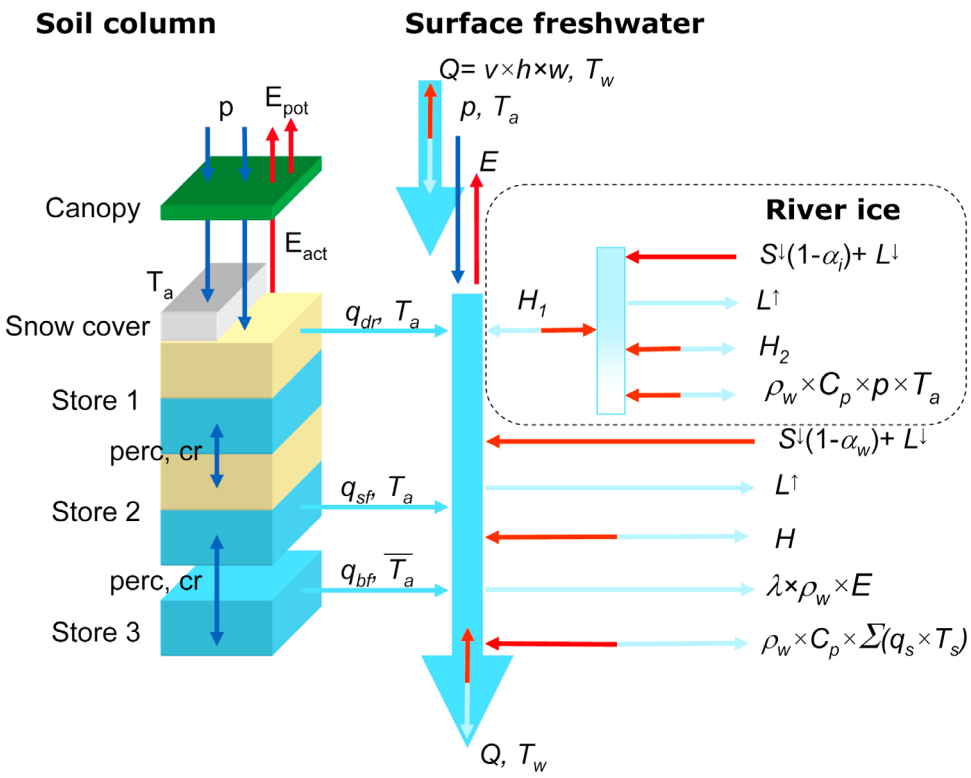

Figure 1. Model concept of PCR-GLOBWB (modified after *van Beek and Bierkens* [2011]). The left-hand side represents the vertical structure for the soil hydrology, representing the canopy, soil column (stores 1 and 2), and the groundwater reservoir (store 3). Precipitation (p) falls as rain if air temperature (T_a) is above 0°C and as snow otherwise. Snow accumulates on the surface, and melt is temperature controlled. Potential evaporation (E_{pot}) is modified by canopy interception and soil moisture to return the actual rate (E_{act}). Vertical transport in the soil column arises from percolation (perc) or capillary rise (cr). Drainage from the soil column to the river network occurs via direct runoff, interflow or subsurface stormflow, and base flow (q_{dr}, q_{sf}, and q_{bf}, respectively). The right-hand side represents the freshwater surface with its inputs (channel discharge Q and direct gain and losses due to rainfall p and evaporation E) and its energy balance. The bounded box represents the modified energy balance if river ice is present. Red-blue arrows represent the energy input with the associated components as explained in equation (1), both local and lateral due to streamflow. Precipitation and specific runoff, which contribute locally to the streamflow, advect energy, which is indicated by the corresponding temperature (air temperature for precipitation, direct runoff, and subsurface stormflow and mean annual temperature for the base flow).

[*New et al.*, 2000] but downscaled using the ERA-40 reanalysis data [*Uppala et al.*, 2005]. Monthly fields of reference potential evapotranspiration were computed according to the FAO guidelines [*Allen et al.*, 1998] from the secondary variables of the CRU TS 2.1 and supplemented with monthly wind speed fields from the CRU CLIM 1.0 data set [*New et al.*, 1999] and downscaled on the basis of ERA-40 daily temperature fields. This study focuses on the results for the subperiod 1976–2000 in which most temperature observations are concentrated.

2.2. Energy Balance Model of Surface Water

[7] We model the energy balance of water with constant density flowing through a rectangular channel with perfect vertical mixing at a daily time step using an explicit numerical scheme and taking the regular grid with a spatial resolution of 0.5° as a Eulerian frame of reference (Figure 2). Streams are intersected by lakes and reservoirs which are treated as continuous and uniform water bodies. These water bodies are represented by a water layer of variable depth that forms as a result of the balance between inflow and outflow and for which the energy balance determines the resulting water temperature. We assume that lateral heat transport occurs by advection only, which is a reasonable assumption for most of the larger rivers with high flow velocities [*Sinokrot and Stefan*, 1993]. Also, we do not take the streambed heat flux into account, as it is assumed small when considering stream water temperature on a daily basis or for longer time steps [*Hondzo and Stefan*, 1994]. Energy fluxes due to friction are small and likewise neglected [*Hicks et al.*, 1997; *Ashton*, 1986]. The resulting surface water energy balance (in J m^{-2} s^{-1}) at a location along the river per unit width, w (m) for a rectangular channel, is then described as (x [L] is coordinate along the drainage network, t is time [T]):

$$\rho_w C_p \frac{\partial(hT)}{\partial t} = -\rho_w C_p \frac{\partial(vhT)}{\partial x} + S^{\downarrow}(1-\alpha_w) + L^{\downarrow} - L^{\uparrow} - H - \lambda\rho_w E + \rho_w C_p \sum_{i=1}^{M} q_{s,i} T_{s,i} \quad (1)$$

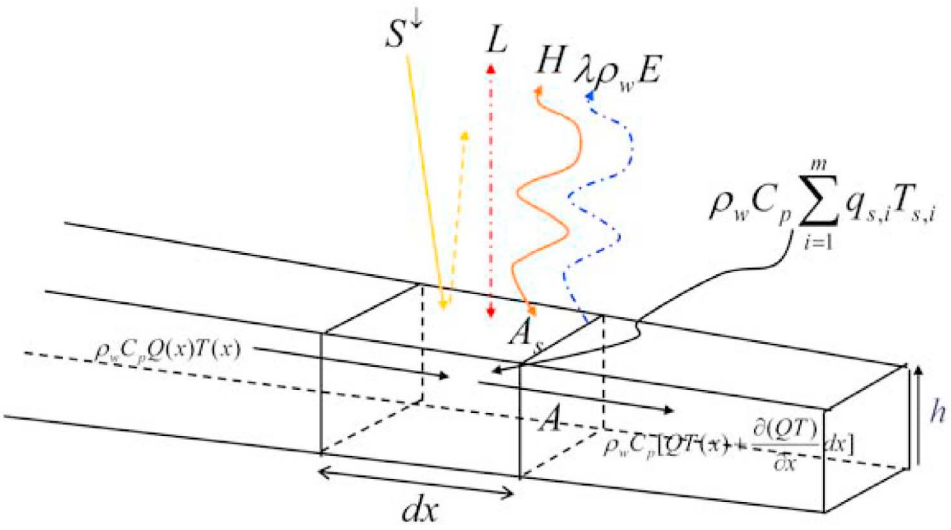

Figure 2. Schematic representation of the energy balance of a rectangular channel. Q represents the streamflow with the associated temperature across a reference volume $A \cdot dx$, with energy being exchanged vertically over the surface area A_s.

where T is average freshwater surface temperature (K); h is water height (m), following from the solution of the kinematic wave equation; ρ_w is density of water (1000 kg m^{-3}); C_p is the heat capacity of water (4190 J kg^{-1} K^{-1}); v is average flow velocity (m s^{-1}) at a point along the channel as follows from the kinematic wave equation; and $S^{\downarrow}$ is the incoming shortwave radiation (J s^{-1} m^{-2}). Here α_w is the albedo of water, and we assumed $\alpha_w = 0.15$; in case of an ice cover it is replaced by $\alpha_i = 0.8$ (assuming that a snow cover is present on the ice floor). $L^{\downarrow}$ is incoming longwave radiation (J s^{-1} m^{-2}) calculated from atmospheric temperature T_a (K), vapor pressure, and cloud cover following *Allen et al.* [1998]. $L^{\uparrow}$ is the outgoing longwave radiation (J s^{-1} m^{-2}), calculated with Boltzmann's equation: $L^{\uparrow} = \varepsilon\sigma T^4$, where T is the water temperature or ice temperature in case of ice cover. The emissivity for both cases is taken as $\varepsilon = 1$. H is the sensible heat flux (J s^{-1} m^{-2}), calculated as

$$H = K_H(T - T_a), \tag{2}$$

where T_a is atmospheric temperature at 2 m height (K) and K_H is the turbulent heat exchange coefficient, which is taken 20 J s^{-1} m^{-2} K^{-1}. In case an ice cover is present, two sensible heat fluxes are considered in series: one from the water to ice surface (assumed to be at 0°C or 273 K) with K_H = 8 J s^{-1} m^{-2} K^{-1},

$$H_1 = K_H(T - 273), \tag{3a}$$

and one from ice surface to the atmosphere with K_H = 20 J s^{-1} m^{-2} K^{-1},

$$H_2 = K_H(273 - T_a); \tag{3b}$$

$\lambda\rho_w E$ is the latent heat flux (J s^{-1} m^{-2}), with E being open water evaporation (m s^{-1}) and λ being the latent heat of vaporization (250 kJ kg^{-1} K^{-1}). The latent heat flux is assumed zero in case of an ice cover.

[8] In line with the routing scheme, the freshwater surface energy balance is evaluated over relatively small time steps using constant rates of vertical inputs of water and energy. To solve for the energy balance, first the vertical changes in the energy balance per cell and then the lateral transport along the drainage network are evaluated. For the time derivative of the vertical energy balance, a forward-difference scheme is used, the change in heat storage for the current time step being directly proportional to the rates of vertical energy exchange and the change in storage. The lateral exchange, which includes both a spatial and temporal derivative, is considered next. Advected heat is associated with the discharge from the kinematic wave approximation along the drainage network for the current time step using a backward finite difference scheme [*Chow et al.*, 1988].

[9] The last right-hand term in equation (1) represents the various water fluxes adding to the water body thereby influencing its energy content, all per unit surface water area A_s (m^2). We do not carry a soil and atmospheric energy balance in PCR-GLOBWB, so the following assumptions are made with regards to the energy advected by lateral inflow: precipitation p (m·s^{-1}) has the same temperature as the atmosphere T_a, which also holds for the direct runoff component q_{dr} (direct runoff m s^{-1}) and q_{sf} (stormflow or interflow m s^{-1}). Further, we assume that groundwater runoff or base flow q_{bf} (m s^{-1}) has a constant temperature equal to the yearly average 2m temperature $\overline{T}_a$ and that none of the respective components can enter at a temperature below the freezing temperature of 0°C. If $f_w = A_w/A$ is the area fraction water in a PCR-GLOBWB cell of size A, then, with the assumption about the temperature of specific runoff components and precipitation, the last right-hand term is given by

$$\rho_w C_p \sum_{i=1}^{M} q_{s,i} T_{s,i} \equiv \rho_w C_p \left\{ pT_a + \left[\frac{1 - f_w}{f_w}\right] \left(q_{dr} T_a + q_{sf} T_a + q_{bf} \overline{T}_a\right) \right\} \tag{4}$$

[10] Any additional anthropogenic influences such as cooling water from power plants, processing water from

Table 1. Overview of Data Sets Used to Verify the Global Surface Water Temperature Model[a]

Variable	Source	Temporal Resolution	Extent	Period
Discharge	GRDC	Daily	Global	Variable, >10 years
Discharge + temperature	USGS	Daily	Conterminous USA	1975–2004
Temperature	NOAA	Daily	Great Lakes (USA, Canada)	1960–1990
Temperature	GEMS	Monthly climatology	Global	1980–2005

[a]Extent pertains to the spatial coverage of the available stations.

industrial activities or sewage water can be easily accounted for by including these terms in (4) but are presently omitted in this study.

[11] Many lakes and rivers are situated in areas where temperatures are below zero for considerable fractions of the year. Consequently, we evaluate the water energy balance together with that of a potential or actual ice cover. Ice will form or grow if the air temperature is below freezing point and is not balanced by the sensible heat flux coming from the water or by the incoming net radiation. The temperature of the ice is kept at 0°C throughout. Any additional cooling results in an increase in ice thickness and a reduction in water temperature until it freezes completely when its temperature reaches 0°C. The change in ice thickness z_i (m) as a result of direct heat inputs to the ice cover over a time step is calculated by

$$\lambda_f \rho_w \frac{dz_i}{dt} = -H_1 + H_2 - S^{\downarrow}(1-\alpha_i) - L^{\downarrow} + L^{\uparrow} \quad (5)$$

where λ_f is the latent heat of fusion of ice (333.4 kJ kg^{-1}).

[12] The formation of ice will have considerable impact on the hydraulic properties of the river; for each river segment, the channel and associated floodplain is represented by a composite, constant width for an assumed rectangular channel and a uniform Manning's roughness coefficient [*van Beek et al.*, 2011]. This width was defined as the minimum of the area as river and floodplain specified by the GLWD3 data [*Lehner and Döll*, 2004] and the area flooded by water levels 1 m above the stage at bankfull discharge for the DEM of the Hydro1k data set [*Verdin and Greenlee*, 1996] in a cell, divided by river length. The corresponding roughness (Manning's n) was computed relative to the wetted perimeter, P, for a stage of 1 m over bankfull discharge using a typical Manning's n of 0.04 for the actual channel and 0.10 for the floodplain. If an ice cover is present, the wetted perimeter of the rectangular channel is further modified from (h water height [L], W channel width [L]) $P = 2h + W$ to $P = 2(h + W)$. Moreover, the ice surface is often rough with typical Manning's n values between 0.01 and 0.10, and a composite Manning's roughness coefficient n_c is calculated for the ice-covered channel according to [*U.S. Army Corps of Engineers*, 2002]

$$n_c = \left(\frac{n_i^{3/2} + n_b^{3/2}}{2} \right)^{2/3} \quad (6)$$

where n_i and n_b are the Manning's n values for the ice cover and the bed respectively. Power functions have been used to establish empirical relationships between water height, ice thickness and roughness coefficients [*Nezhikovskiy*, 1964]. These show a decreasing roughness with water height and an increasing roughness with ice thickness for different ice types (thick and thin ice jams and frozen-up covers with decreasing roughness). These functions for n_i can be approximated by a general function which is applied here:

$$n_i = 0.0493 h^{-0.23} z_i^{0.57} \quad (7)$$

[13] The influence of ice on river discharge is considerable. If we assume that the flow area remains constant and that bed and ice roughness are equal, the increase in the wetted perimeter alone reduces the hydraulic radius by 50% if the width of the channel is large compared to the flow depth, thus resulting in a 37% decrease in flow velocity.

3. Data and Validation Results

[14] The ability of PCRGLOB-WB to simulate river discharge was validated extensively in *van Beek et al.* [2011]. Validation was based on all stations (N = 1983) from the *Global Runoff Data Centre* (*GRDC*) [2011] long-term global river runoff data set with time series exceeding 10 years over the observation period. Here we repeat the main conclusion that PCR-GLOBWB is able to reproduce the within year and between year variability of discharge of the major rivers adequately, where results are better for the larger rivers and for rivers with larger effective rainfall. In terms of reproducing absolute values of river discharge, results very much depend on the quality of the meteorological forcing. As a result, good results are found for the rivers in Europe and the United States, where the CRU rainfall maps are based on many rain gauges and ERA-40 reanalysis data are of high quality due to the ingestion of abundant data during reanalysis. For the same reason, i.e., the lack of CRU stations and little data to ingest during reanalysis, precipitation in CRU and ERA-40 across South America and Africa are of limited quality [*Biemans et al.*, 2009] resulting in an underestimation of the Amazon discharge and an overestimation for African rivers such as the Congo, Zambezi, the Orange and the Nile. Finally, underestimation of discharge peaks of arctic rivers occurs due to the snow undercatch in the CRU TS 2.1 and the simplified representation of snow hydrology in PCR-GLOBWB. For a more in depth evaluation of model performance of PCRGLOB-WB of discharge we refer to *van Beek et al.* [2011].

[15] To validate the simulations of surface water temperature we use the temperature data sets as reported in Table 1. To test the reproduction of long-term average yearly and monthly temperatures we used the GEMS/Water (http://www.gemswater.org/) monthly climatology data. In this data set spatial and temporal coverage by stations is highly variable and we retrieved from this data set 296 stations with full or partial information on the long-term mean monthly water temperature by extending our selection criteria to the period 1980–2005. Of these stations, 288 stations have information on upstream area and for 149 stations the climatology contains more than 9 months and the difference between the reported

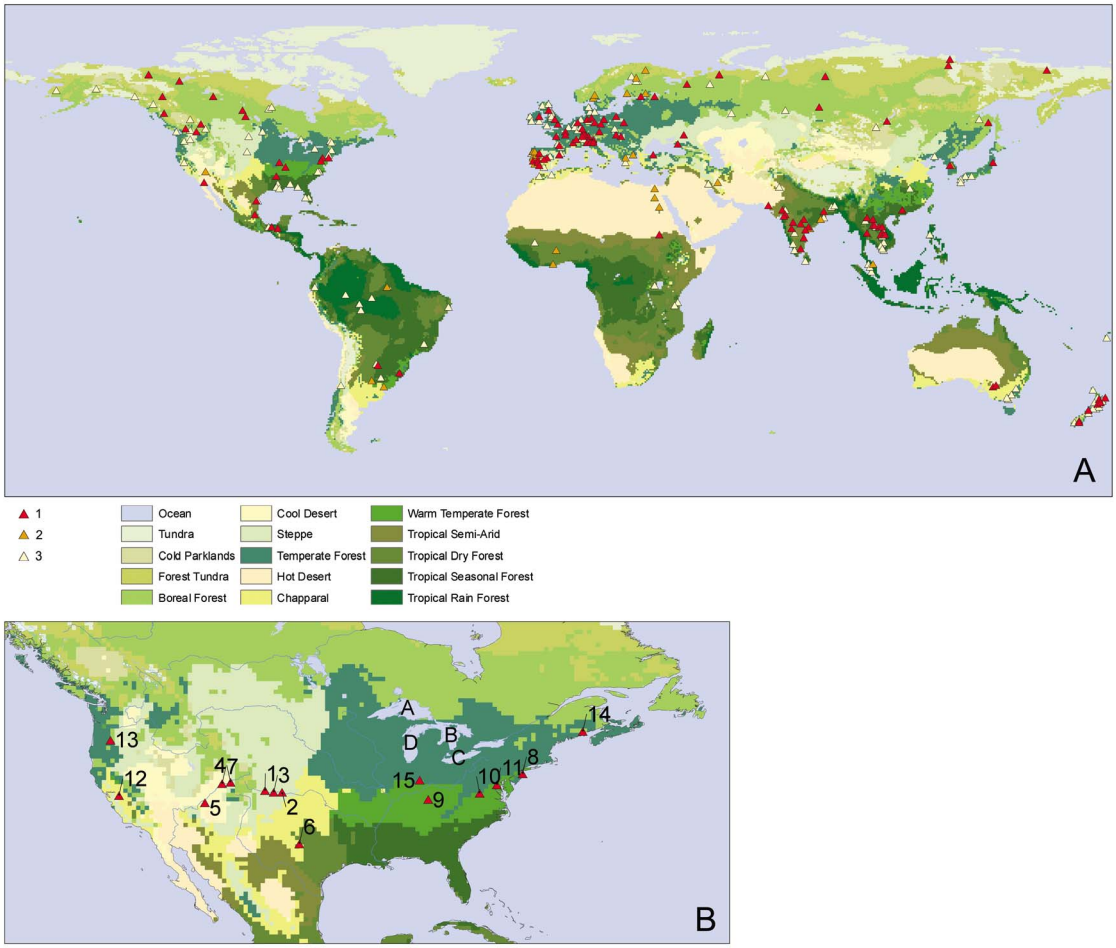

Figure 3. Stations with water temperature observations. (a) Stations from the GEMS database with monthly climatology: (1) GEMS stations with a climatology of 9 months or more based on more than 5 years of water temperature data, with an absolute catchment of less than 10%, and linked to GRDC discharge data (N = 114), (2) same as type 1, but relaxing the conditions of more than 5 years of water temperature data and the availability of GRDC discharge (N = 149), and (3) all GEMS stations with temperature information (N = 296). (b) USGS stations and NOAA lake data set with daily temperature data, as numbered according to Table 2: 1: Arkansas above Pueblo; 2: Arkansas John Martin Reservoir; 3: Arkansas Las Animas; 4: Colorado Cameo; 5: Colorado Lees Ferry; 6: Colorado Silver; 7: Colorado Utah Stateline; 8: Delaware at Trenton; 9: Green River Campbellsville; 10: Jackson River; 11: Potomac near Washington; 12: San Joaquin Vernalis; 13: Mackenzie South Fork; 14: St. Croix Milltown; 15: White River Centerton; A: Lake Superior; B: Lake Huron; C: Lake Erie; D: Lake Michigan. Stations are superimposed on the Holdridge life zone classification [*Leemans*, 1989].

upstream area and that included in the model is less than 10%. Of these stations, 114 stations can be linked to GRDC discharge measurements and represent more than 5 years of temperature data (Figure 3a). The stations are plotted against the backdrop of the *Holdridge* [1967] life zone classification with a spatial resolution of 0.5° [*Leemans*, 1989]. The Holdridge life zone classification is used to check whether the accuracy of temperature simulation varies over climate zones, and to check how differences between water temperature and atmospheric temperature through the year vary between climate zones. Daily simulations of surface water temperature were compared to a limited number of stations available in the USA: the USGS (Water data for the nations, http://waterdata.usgs.gov/nwis) daily river temperature and discharge data set (period 1975–2004 for 15 stations) and NOAA Great Lakes temperature data (1960–1990 for four lakes; http://www.glerl.noaa.gov/res/glcfs; Figure 3b).

[16] In the subsequent analyses, a several statistics are used to summarize the data and to evaluate model performance. These include the mean error, mean absolute error and relative error, all with reference to observed values; the Nash-Sutcliffe efficiency; the regression coefficient or slope of a linear regression line forced through the origin and, the correlation coefficient of a regular linear regression of the observed values on the simulated ones.

3.1. Mean Monthly Water Temperature

[17] We compared the GEMS monthly climatology of water temperature with the simulated one. Figure 4a shows for each GEMS station the mean deviation in water temperature

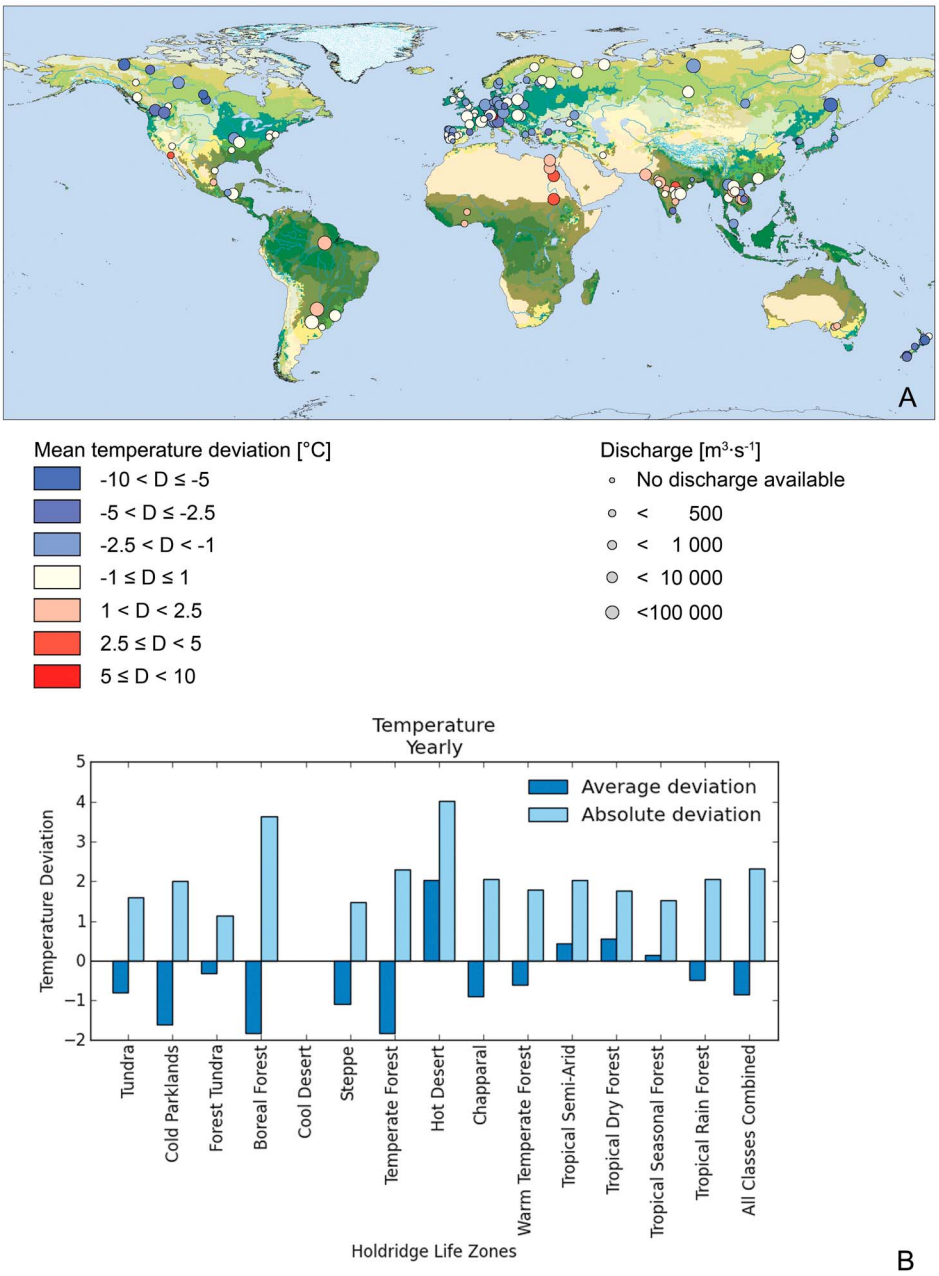

Figure 4. Deviations between observed and simulated temperature. (a) Mean average deviation (°C) per station climatology (N = 149) with symbol size proportional to observed discharge. Warmer colors indicate an overestimation; cooler colors indicate an underestimation of the observed temperature. (b) Mean absolute and average deviation (°C) per Holdridge life zone for all available data. Number of stations per Holdridge life zone is as follows: tundra, 1; cold parklands, 2; forest tundra, 4; boreal forest, 23; cool desert, 0; steppe, 3; temperate forest, 48; hot desert, 7; chapparal, 12; warm temperate forest, 9; tropical semiarid, 8; tropical dry forest, 15; tropical seasonal forest, 12; tropical rain forest, 5; all classes combined, 149.

where the size of a circle is proportional to the observed discharge at the station. Figure 4b shows the mean and mean absolute monthly deviation per Holdridge life zone. Errors are generally small (mean absolute error across all stations = 2.3°C, N = 149). Results are slightly better for locations with larger discharge as runoff across larger basins is better captured by the large-scale hydrological model [*van Beek et al.*, 2011] (see also Figure S1 in the auxiliary material).[1]

[18] Figure 4 shows that water temperatures are generally underestimated by 0.5 to 5°C in some of the northwestern

[1]Auxiliary materials are available in the HTML. doi:10.1029/2012WR011819.

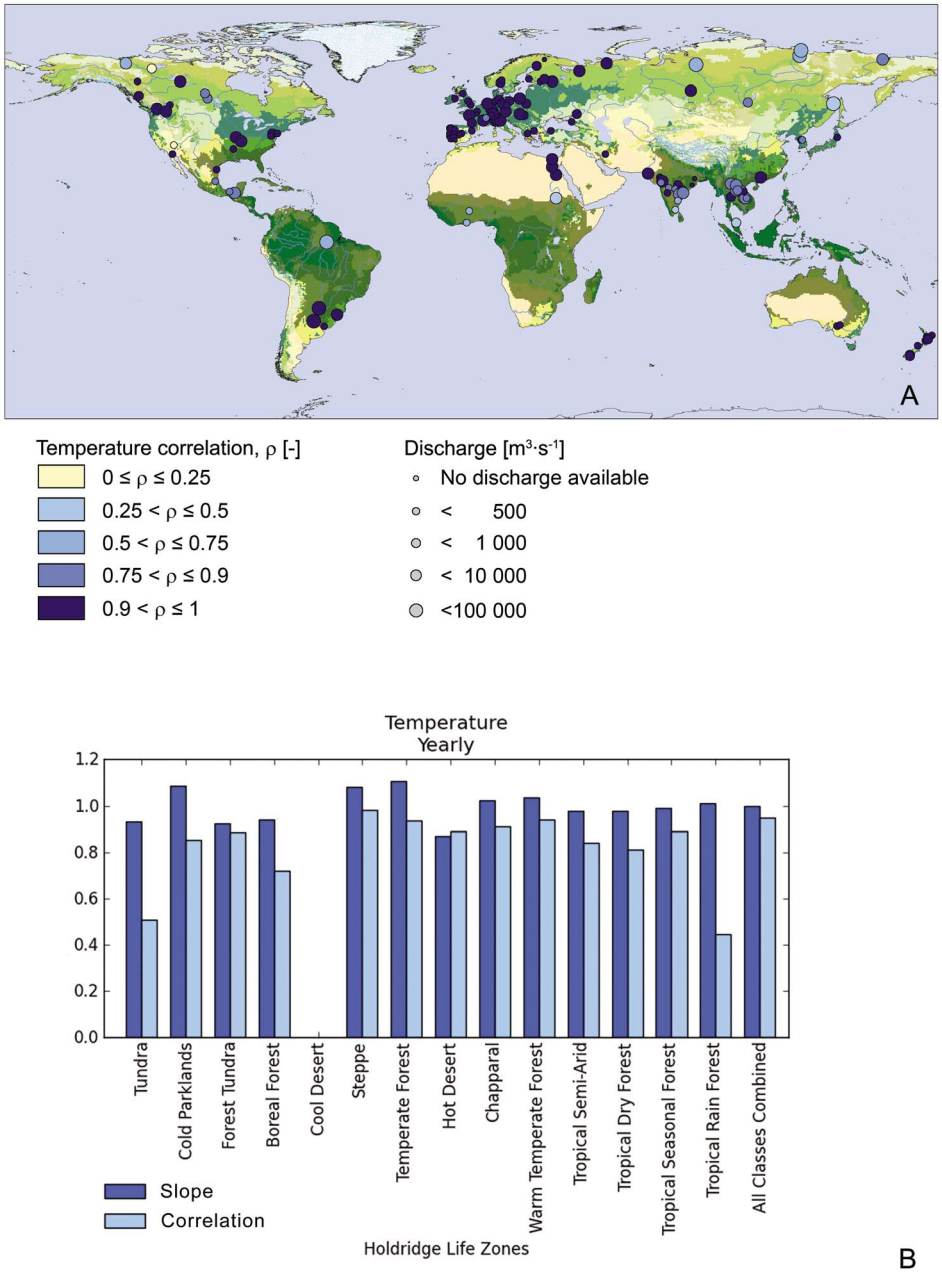

Figure 5. Regression of observed on simulated water temperature: (a) correlation coefficient per station climatology (N = 134), with symbol size proportional to observed discharge, and (b) correlation coefficient per Holdridge life zone and the slope where the trend line is forced through the origin for all available data (see Figure 4 for number of stations per Holdridge life zone).

European rivers (Rhine, Po, Ebro). This underestimation is most likely caused by neglecting the effects of the use of river water for cooling of power plants and factories. Even though the mean absolute errors are on average a few degrees centigrade (Figure 4b), it is clear that they are strictly positive in the wet African, Southeast Asian, and South American tropics. Possible causes for this overestimation of water temperature are the underestimation of water albedo and emissivity or the overestimation of incoming radiation, most likely due to the neglect of shading of the tropical forest canopy for the smaller streams. Also, the assumption that rainfall has the same temperature as the atmosphere may not be valid. Much of the tropical rainfall occurs in deep convection thunderstorms where rainfall is formed very high up in the atmosphere yielding rainwater temperatures that are lower than the atmospheric temperature observed close to the land surface. Unfortunately, little is known about the difference between the temperature of rainfall and that of the lower atmosphere. Observations [*Byers et al.*, 1949] and theoretical analysis [*Kinzer and Gunn*, 1951] seem to suggest that raindrops, while freely falling, behave like a wet bulb and the temperature difference can be calculated from atmospheric temperature and relative humidity. However, *Byers et al.* [1949] also observe that the temperature difference diminishes quickly during a

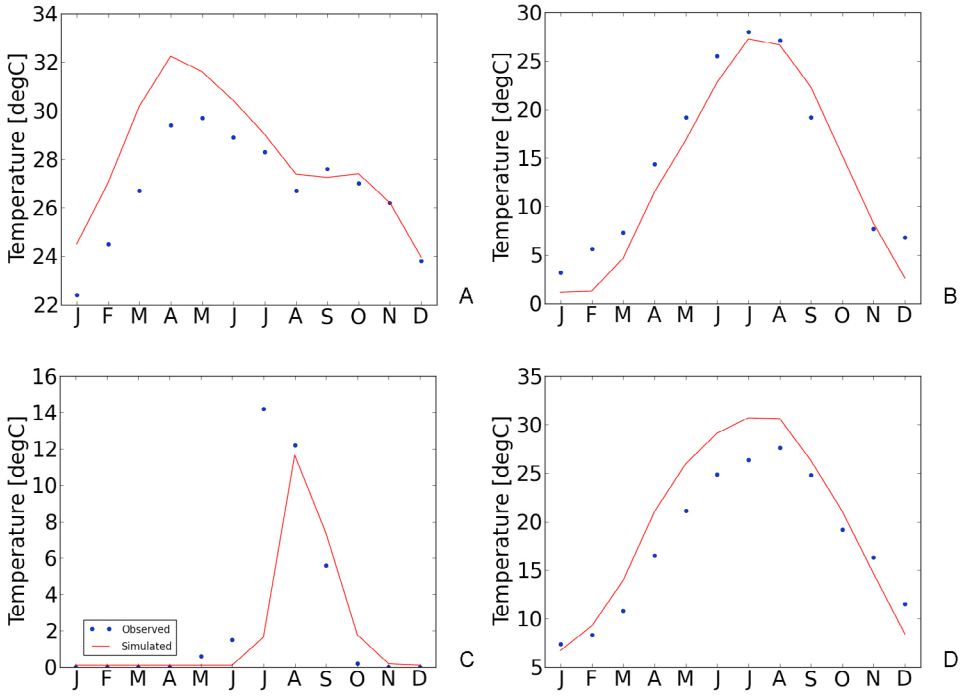

Figure 6. Monthly climatologies of freshwater surface temperatures for (a) Mekong River, Nakhon Phano (GRDC station 2969095), (b) Missouri River, Missouri (GRDC station 4122900), (c) Lena River, Kusur (GRDC station 2903420), and (d) Yangtze River (Chang Jiang; GRDC station 2181600).

rainstorm, most likely due to increasing relative humidity if rainfall persists. A straightforward way to estimate rain temperature from meteorological data sets such as ERA-40 and CRU is therefore not available. Instead, we performed a sensitivity analysis by rerunning the model assuming that rainfall and direct runoff have a water temperature that is 1.5°C lower than atmospheric temperature. Results from this run show a reduced bias in water temperature over the tropics although this improvement is limited (see Figure S2 in the auxiliary material).

[19] Figure 5a shows for each GEMS station the correlation coefficient between observed and simulated mean monthly temperatures. In Figure 5b the results are summarized by a bar chart for the different climate zones. In addition to the correlation coefficient, the slope, α, of a regression that is forced through the origin is shown, which preferably should coincide with the 1:1 line ($|\alpha| = 1$). Generally the correlation coefficient is positive and close to unity for all stations and across climate zones. Similarly, the slope is close to one, suggesting that the model is capable of reproducing the seasonal trend in water temperature and the associated means. Notwithstanding, statistics for the tropics as well as in the arctic areas are somewhat lower. The former is caused by the lack of a strong seasonal signal, making the signal-to-noise ratio and thus the explained variance lower (e.g., Mekong in Figure 6). The reduced performance for the subarctic climate zones can be attributed to the difficulty in simulating the start and ending of the ice cover (e.g., Lena in Figure 6). In particular the ending of the ice period is not represented well as the model simulates only ice melt and not the mechanical breakup. This causes the temperature to rise too late in spring. In Figure 7 scatterplots are shown for simulated and observed surface water temperatures, where symbols represent the different climate zones. Winter (DJF) results are generally good, while the summer (JJA) results show larger deviations in particular for the colder climate zones, again suggesting a simulated temperature rise that is too late.

3.2. Daily Water Temperature

[20] Daily temperature time series from the USGS data set (period 1975–2004 for 15 river stations; http://waterdata.usgs.gov/nwis) and NOAA Great Lakes data set (1960–1990 for 4 lakes; http://www.glerl.noaa.gov/res/glcfs) were compared to daily temperature simulations from a data set. Figure 8 shows time series for three USGS locations, and Figure 9 shows time series for the Great Lakes. For clarity only a 10 year period is shown for which the most data-rich period was chosen (1991–2000 for the USGS river stations, 1981–1990 for the NOAA lake stations). Comprehensive statistics on performance are shown in Table 2 for all available stations. Performance is less consistent than for the monthly climatologies from the GEMS data set. For the USGS daily river data the most probable cause for this is the error in catchment size (e.g., Mackenzie at South Fork, Jackson River). The upstream catchments size of many of the data is small compared to the 0.5° × 0.5° grid size of PCR-GLOBWB and the resulting error can cause substantial deviations in discharge, total water volume stored and the timing of daily discharge. This in turn will cause both systematic and timing errors in water temperature, albeit much smaller than the errors in discharge. When daily results are aggregated to a coarser temporal resolution, performance improves; timing at the monthly time scale is better than at the daily time scale and better for the monthly climatology still (Table 2). Results for the monthly climatology approach those for the GEMS stations.

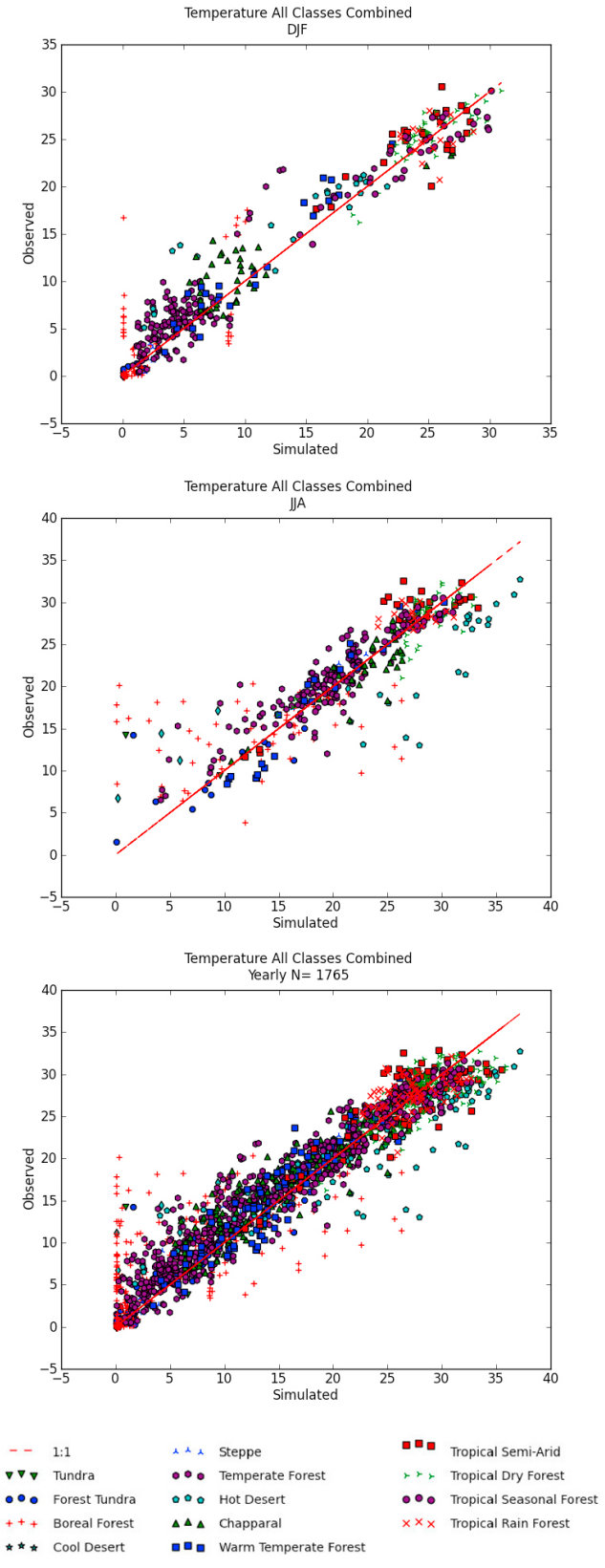

Figure 7. Scatterplots of observed versus simulated monthly water temperature for winter (DJF: December, January, February) and summer (JJA: June, July, August) and for the entire year.

[21] While good agreement of the seasonal temperature signal is evident and trivial, the ability of the model to simulate interannual variability for the current climate is of particular importance when using the model to study the impacts of climate change. The correlation on yearly averaged water temperature shows smaller correlations are found than for the monthly and daily temperatures since the seasonal variation has been removed [*Erickson and Stefan*, 2000]. However, the correlations are still considerable showing that interannual variation is captured reasonably well providing confidence that the model captures water temperature variations over a range of temporal scales accurately.

[22] Regression coefficients and especially Nash-Sutcliffe model efficiencies test for bias in modeled water temperature. Out of the 15 stations, 8 have a NSE equal or greater than 0.48, indicating fair (NSE≥0.5) to good model performance. Overall, deviations in the slope from the 1:1 line tend to be small. Notable exceptions are those stations with large errors in catchment size and the stations associated with reservoirs (Arkansas at John Martin reservoir, Colorado at Lees Ferry). Here, mixing occurs apparently over a larger volume than the active water depth represented by the model. An obvious improvement therefore would be to consider different mixing types depending on the outlet position (e.g., tailwaters fed by under or overflow).

[23] Similarly, errors in lake temperatures result from the neglect of surface currents and vertical stratification in the model, including the seasonal overturning of the epilimnion. To check whether any improvements can be expected when vertical stratification and overturning are modeled, we also applied a designated water temperature model for lakes (FLake [*Mironov*, 2008]). Upon calibration and application (see Figure S4 and Table S1 in the auxiliary material), we did not find this model to outperform PCR-GLOBWB consistently. We can only speculate about this lack of improvement but possibly the larger number of parameters necessary to run FLake cause additional uncertainty, requiring better data or an even more sophisticated lake model to make the difference.

4. Seasonal Temperature Differences

[24] The large heat capacity of water, particularly when frozen, and the lateral transport of energy through rivers can result in large differences between surface water and air temperature. In Figure 10 the average temperature difference between surface water and air temperature is plotted for the various Holdridge life zones. As expected, the maximum variation of this deviation occurs in the colder climate zones, which are predominantly found at higher latitudes and altitudes in the Northern Hemisphere (tundra, cold parklands, forest tundra, boreal forest). A regional picture of seasonal differences between water and air temperature shows many different features (Figure 11): for instance, one observes water being warmer than the atmosphere in the Northern Hemisphere in boreal winter (DJF), being colder in spring when the atmosphere heats up (MAM for the lower latitudes, JJA for higher latitudes and more continental climate zones) and then heating up at a slower pace than the atmosphere during boreal summer (JJA). The influence of meltwater on river water temperature is apparent in the case of the Danube, Mississippi, Volga, St. Lawrence in spring (MAM), and in early summer (JJA) of the Mackenzie, Yenisei, and

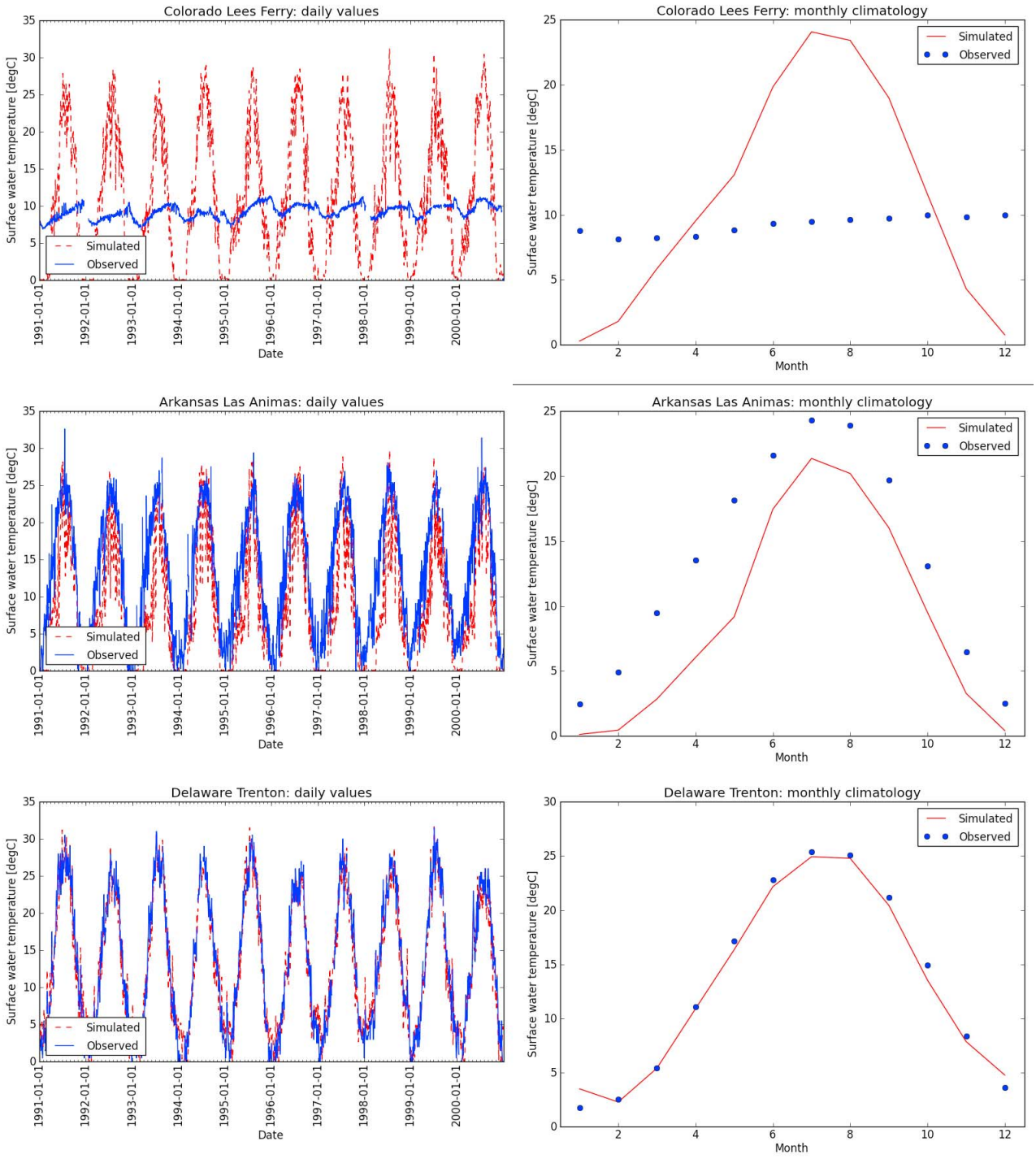

Figure 8. Time series of freshwater surface temperatures for three USGS stations with daily observations. The stations with the lowest, median, and highest Nash-Sutcliffe efficiency were selected (see also Table 2), ordered by increasing model performance from top to bottom. Daily observations over a selected 10 year period and the monthly climatology computed from all available data are shown.

Lena River and the upper reaches of the Asian rivers springing from the Himalayas. The Nile represents another interesting case as during the low-flow period, the White Nile transports warmer water from the tropics to the north, but in August, when the rains occur in the Ethiopian highlands, colder water from the Blue Nile decreases the water temperature over a few hundreds of kilometers (JJA). As can be seen, the temperature of the tropical rivers in South America and Africa is higher than daily average temperature throughout the year. Although other authors have reported consistently higher surface water temperatures than 2 m average daily temperature for tropical rivers (see, e.g., *van Vliet et al.* [2011] for the Parana), overestimation of surface water temperature due to overestimation of precipitation

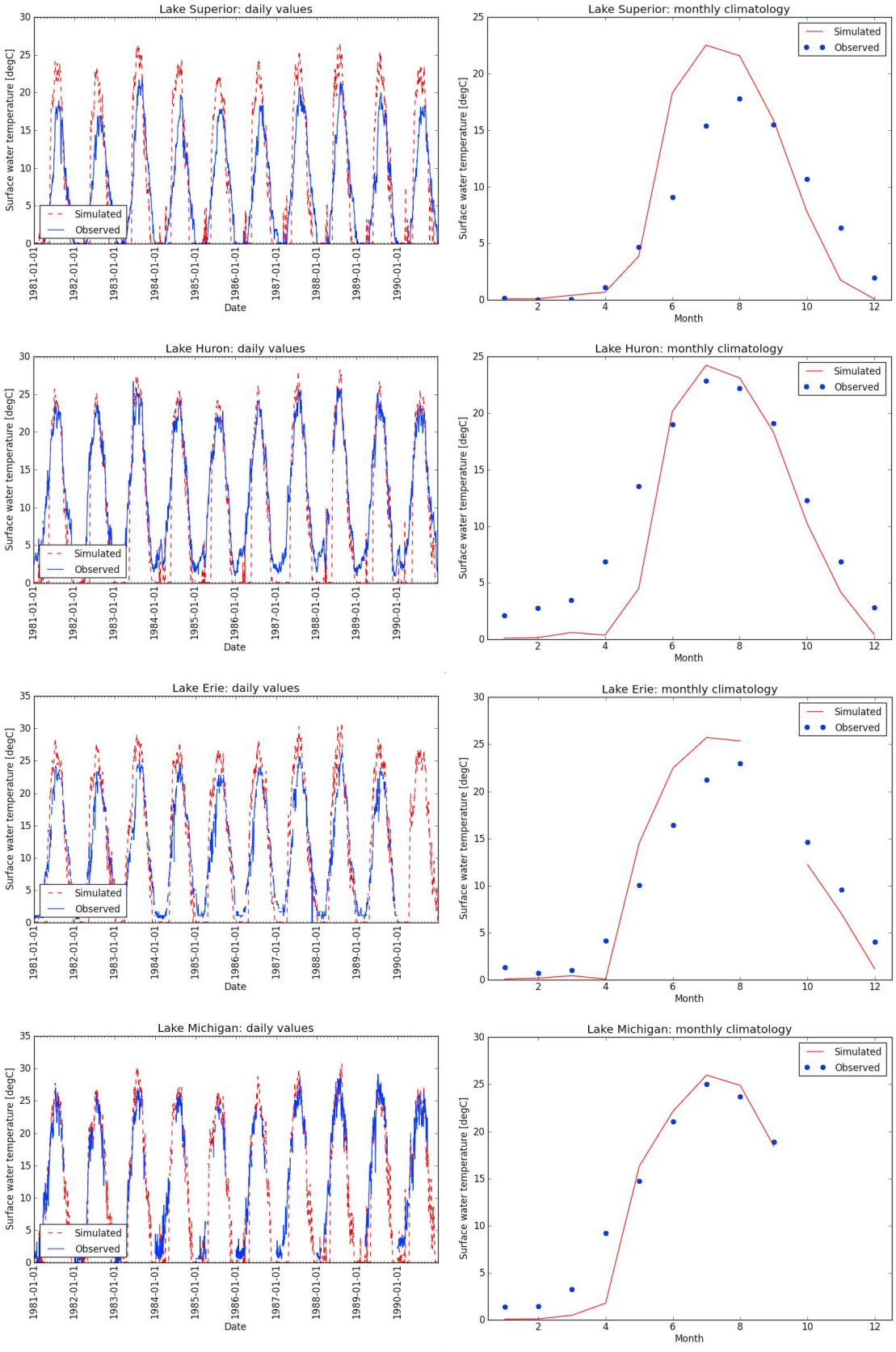

Figure 9. Time series of freshwater surface temperatures for the NOAA stations from the Great Lakes data set. The stations with the lowest, median, and highest Nash-Sutcliffe efficiency were selected (see also Table 2), ordered by increasing model performance from top to bottom. Daily observations over a selected 10 year period and the monthly climatology computed from all available data are shown.

Table 2. Relative Error in Catchment Size (REA), Mean Error (ME), Mean Absolute Error (MAE), Nash-Sutcliffe Efficiency (NSE), and Coverage (COV), Slope (α), and Correlation (ρ) for the Daily, Monthly, and Yearly Values and for the Monthly Climatology[a]

Station	Name	Area (km^2)	REA	ME (°C)	MAE (°C)	NSE	Daily			Monthly			Monthly Climatology			Yearly		
							COV	α	ρ	COV	α	ρ	COV	α	ρ	COV	α	ρ
USGS Rivers and Station Names																		
1	Arkansas above Pueblo	12,142	59.5%	−4.0	4.8	0.191	51%	1.129	0.838	42%	1.212	0.894	42%	1.209	0.909	36%	1.532	0.803
2	Arkansas John Martin Reservoir	49,179	8.9%	−1.2	4.2	0.331	51%	0.886	0.844	42%	0.947	0.898	42%	0.946	0.913	36%	1.124	0.796
3	Arkansas Las Animas	37,484	−2.9%	−4.5	4.7	0.483	51%	1.213	0.890	38%	1.279	0.947	38%	1.279	0.965	21%	1.458	0.710
4	Colorado Cameo	20,930	−8.9%	−5.1	5.1	0.189	65%	1.435	0.874	55%	1.519	0.916	55%	1.545	0.928	41%	1.994	0.868
5	Colorado Lees Ferry	290,680	−0.7%	1.7	7.6	−69.658	45%	0.510	0.243	36%	0.530	0.256	36%	0.535	0.346	29%	0.826	−0.033
6	Colorado Silver	38,766	1.1%	−0.9	2.1	0.879	66%	1.022	0.957	55%	1.033	0.983	55%	1.035	0.999	36%	1.059	0.911
7	Colorado Utah Stateline	46,540	19.0%	−4.6	4.8	0.378	36%	1.253	0.888	32%	1.322	0.934	32%	1.343	0.947	28%	1.628	0.898
8	Delaware at Trenton	17,628	5.7%	−0.2	1.6	0.947	85%	1.014	0.973	54%	1.023	0.990	54%	1.027	0.997	32%	1.016	0.991
9	Green River Campbellsville	1,773	39.1%	−0.8	4.2	0.542	24%	1.055	0.744	16%	1.064	0.834	16%	1.061	0.943	6%	1.031	1.000
10	Jackson River	897	171.3%	−1.0	3.2	0.486	83%	1.075	0.723	62%	1.091	0.784	62%	1.114	0.912	40%	1.066	0.566
11	Potomac near Washington	30,056	3.8%	−0.4	2.1	0.912	44%	1.015	0.956	31%	1.036	0.985	31%	1.039	0.997	21%	1.025	0.700
12	San Joaquin Vernalis	35,194	4.9%	−2.4	2.9	0.535	90%	1.097	0.914	77%	1.121	0.954	77%	1.124	0.989	64%	1.155	0.834
13	Mackenzie South Fork	541	310.2%	−1.5	2.9	−0.750	65%	1.027	0.406	55%	1.068	0.452	55%	1.057	0.499	42%	1.199	0.725
14	St. Croix Milltown	3,783	−42.3%	−4.7	6.7	0.238	67%	1.830	0.873	49%	1.880	0.932	49%	1.812	0.947	23%	1.611	0.967
15	White River Centerton	6,354	11.9%	−1.3	2.3	0.865	71%	1.049	0.946	49%	1.079	0.974	49%	1.089	0.996	27%	1.130	0.610
NOAA Great Lakes																		
A	Lake Superior	NA	NA	0.9	3.2	0.538	59%	0.749	0.895	55%	0.764	0.910	55%	0.766	0.919	55%	0.884	0.642
B	Lake Huron	NA	NA	−2.3	3.1	0.704	57%	0.985	0.934	56%	1.001	0.950	56%	1.007	0.962	51%	1.264	0.778
C	Lake Erie	NA	NA	0.5	3.2	0.747	46%	0.850	0.938	6%	0.861	0.968	6%	NA	NA	3%	NA	NA
D	Lake Michigan	NA	NA	−1.0	2.3	0.864	36%	0.964	0.958	12%	0.963	0.969	12%	NA	NA	0%	NA	NA

[a]Coverage represents the fraction of the period analyzed present in the observations. For daily data, this includes all observations, for monthly data all months that have full daily coverage, and for years those that have 9 or more complete months present. For the climatology, it represents the number of years per month. USGS stations have been relocated to the nearest adjacent cell within the same basin that resulted in the smallest absolute error. For the lakes a relative error in catchment size is not applicable. See Figure 3b for location of the stations.

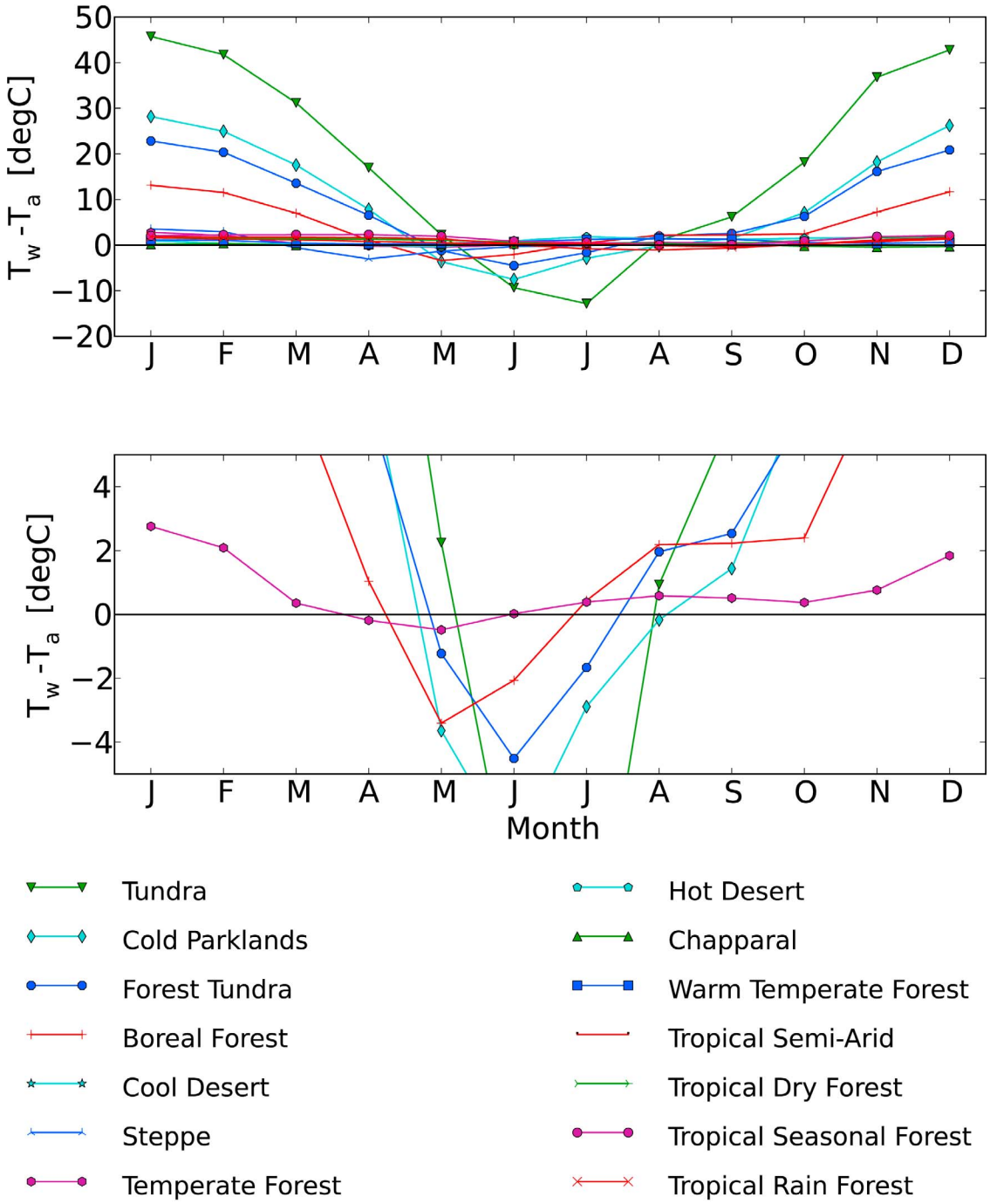

Figure 10. (top) Climatology of the difference between freshwater surface temperature and that of the overlying air ($T_w - T_a$) for the different Holdridge life zones. (bottom) The same data at a reduced vertical scale for a selection of classes.

temperature and radiation (neglecting shading) may play a role here. Figure S3 in the auxiliary material is similar to Figure 11, but now obtained by assuming precipitation and direct runoff that is 1.5°C colder than the 2 m air temperature as discussed above. This leads to lower surface freshwater temperatures in those areas where direct runoff is the main contributor to the specific runoff. However, water temperatures stay consistently higher than the air temperature for the larger rivers in the tropics.

5. Discussion and Conclusion

[25] In this paper we introduced a physically based deterministic model of global surface water temperature based on solving the surface water energy balance driven by

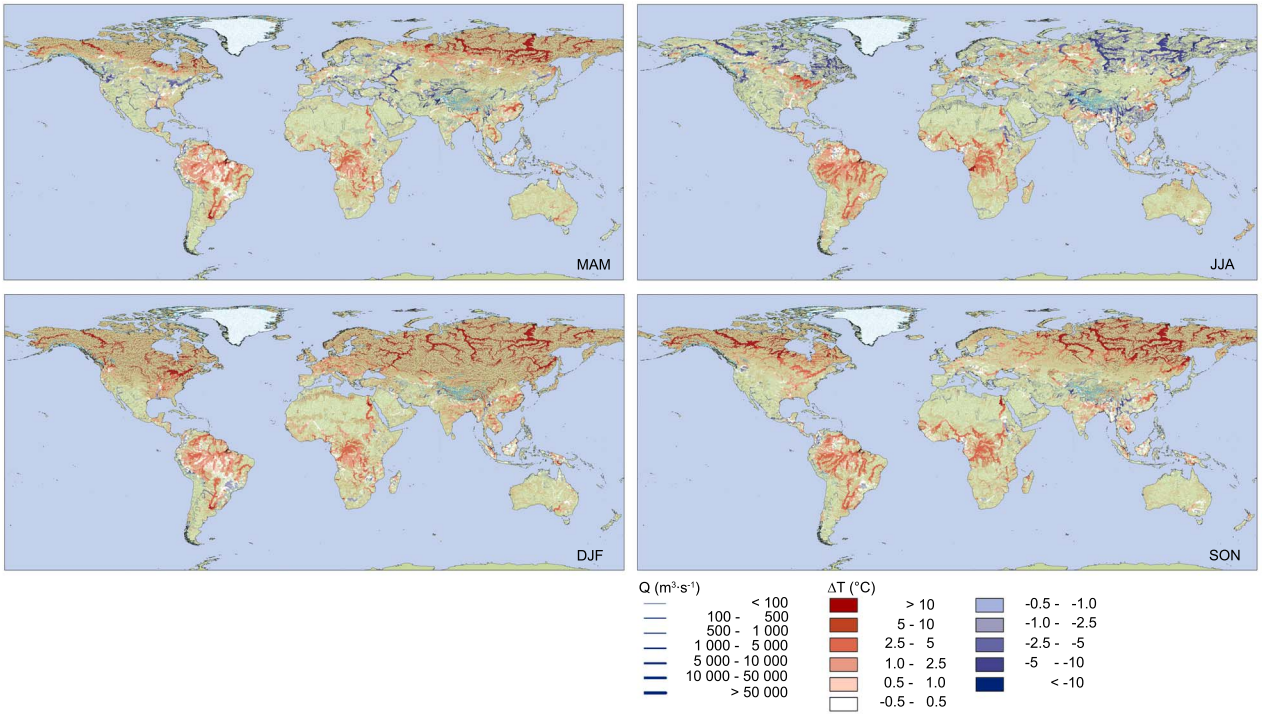

Figure 11. Seasonally averaged difference between surface water and air temperature ($T_w - T_a$) for river stretches around the world (MAM through DJF, clockwise from top left). Thickness of line is proportional to river discharge; warmer colors denote that the fresh surface water is warmer than the overlying air, and cooler colors indicate that it is colder.

radiation, precipitation and temperature from the CRU and ERA-40 data sets and runoff and river discharge fluxes computed with a global hydrological model. The model was parameterized on the best available data and not calibrated on the premise that a strong physical basis makes the model better suited for extrapolation, for instance when analyzing the effects of climate change and increased use of cooling water on the change of surface water regimes. Also, contrary to statistical approaches to modeling water temperature, surface water temperature can be calculated everywhere along the surface water network in a consistent manner and with preservation of the surface water energy balance.

[26] Any comparison to existing deterministic models of freshwater surface temperature has limited validity. Such models are typically applied in regional studies to evaluate the effects of local disturbances and calibrated to match high-quality data sets, often over a limited part of the year [e.g., *Sinokrot and Stefan*, 1993; *Younus et al.*, 2000]. In contrast, the model presented here is applied on a global scale and parameterized using available data sets of varying quality in which local detail is lost and applied continuously over a much longer period (25 years). Moreover, the model is not calibrated but validated directly against observations. Reported prediction errors of deterministic models generally are in the order of 1–2°C [*Caissie*, 2006] and obviously lower than those obtained in this global study where the mean absolute error ranges between 1.6 and 7.6°C for the daily stations (Table 2) and is on average 2.3°C for those with monthly climatologies only (Figure 4). Notwithstanding, given the coarse resolution of the model and the extended period of application, it may be concluded that results show that the model is able to capture well the mean monthly surface temperature for the majority of the GEMS stations both in time and space, while the interannual variability as derived from the USGS and NOAA data was also captured reasonably well. Thus, the model appears to be relatively insensitive to the neglect of shading and the simplifying assumptions that were made with regards to the energy advected by precipitation and runoff, provided that these fluxes and the ensuing discharge are adequately simulated. Calibration will improve model performance but the problem is poorly constrained by the limited availability of global water temperature data and the improved model performance may be obtained for the wrong reasons. Moreover, persistent errors in global precipitation products will propagate through the hydrology and the associated surface water energy balance and severely bias the calibrated parameter set. As such a robust, calibrated parameterization that is consistent with the physical nature of the model remains unachievable until better global precipitation products are available.

[27] Results are poorest for the arctic rivers, possibly because the timing of ice breakup is predicted too late in the year due to the lack of an algorithm describing mechanical ice breakup. Moreover, surface water temperatures for tropical rivers were overestimated, most likely due to an overestimation of rainfall temperature and possibly incoming shortwave radiation. The spatiotemporal variation of water temperature reveals large temperature differences between water and atmosphere for the higher latitudes, while considerable lateral transport of heat can be observed for

rivers crossing hydroclimatic zones such as the Nile, the Mississippi and the large rivers flowing into the Arctic.

[28] Overall, our model results show promise for future projection of global freshwater surface temperature under global change. Possible improvements to the model are the inclusion of a soil energy balance model, shading of surface water by vegetation, explicit modeling of rainfall temperature, and vertical stratification in lakes including epilimnion overturning and mixing in reservoirs. Anthropogenic influences that should be considered are water withdrawal that affects the heat storage capacity of streams and thermal pollution by cooling waters used in power plants and industry, which increasingly upsets the natural thermal regime of surface freshwater bodies in the developed and developing regions of the world.

[29] **Acknowledgments.** We would like to thank Dmitrii Mironov at the German Weather Office (DWD) for providing us with FLake, the water temperature model for lakes. We gratefully acknowledge the United Nations Environment Programme Global Environment Monitoring System (GEMS) for providing us with monthly climatologies of freshwater surface temperature and the Global Runoff Data Centre (GRDC) for the associated discharge. We also wish to express our thanks to the U.S. Geological Survey (USGS) and the NOAA Great Lakes Environmental Research Laboratory (NOAA GLERL) for providing the daily station data for water temperature we used. The contribution of Michelle van Vliet to this study was financially supported by the European Commission through the FP6 Water and Global Change Project (WATCH). We would like to thank the three anonymous reviewers, whose comments have contributed considerably to the clarity and readability of this paper. Simulated freshwater surface temperature and associated variables are publicly available from http://www.globalhydrology.nl/maps/ and can be used freely for research purposes with reference to this publication.

References

Allen, R. G., L. S. Pereira, D. Raes, and M. Smith (1998), Crop evapotranspiration, *FAO Irrig. Drain. Pap. 56*, Food and Agric. Organ., Rome.

Ashton, G. D. (1986), *River and Lake Ice Engineering*, Water Resour. Publ., Littleton, Colo.

Beitinger, T. L., W. A. Bennett, and R. W. McCauley (2000), Temperature tolerances of North American freshwater fishes exposed to dynamic changes in temperature, *Environ. Biol. Fishes*, *58*, 237–275, doi:10.1023/A:1007676325825.

Benyahya, L., D. Caissie, A. St-Hilaire, T. B. M. J. Ouarda, and B. Bobee (2007), A review of statistical water temperature models, *Can. Water Resour. J.*, *32*, 179–192, doi:10.4296/cwrj3203179.

Biemans, H., R. W. A. Hutjes, P. Kabat, B. J. Strengers, D. Gerten, and S. Rost (2009), Effects of precipitation uncertainty on discharge calculations for main river basins, *J. Hydrometeorol.*, *10*, 1011–1025, doi:10.1175/2008JHM1067.1.

Burgmer, T., H. Hillebrand, and M. Pfenningerm (2007), Effects of climate-driven temperature changes on the diversity of freshwater macroinvertebrates, *Oecologia*, *151*, 93–103, doi:10.1007/s00442-006-0542-9.

Byers, H. R., H. Moses, and P. J. Harney (1949), Measurement of rain temperature, *J. Meteorol.*, *6*, 51–55, doi:10.1175/1520-0469(1949)006<0051:MORT>2.0.CO;2.

Caissie, D. (2006), The thermal regime of rivers: A review, *Freshwater Biol.*, *51*, 1389–1406, doi:10.1111/j.1365-2427.2006.01597.x.

Caissie, D., M. G. Satish, and N. El-Jabi (2007), Predicting water temperatures using a deterministic model: Application on Miramichi River catchments (New Brunswick, Canada), *J. Hydrol.*, *336*, 303–315, doi:10.1016/j.jhydrol.2007.01.008.

Chow, V. T., D. R. Maidment, and L. W. Mays (1988), *Applied Hydrology*, McGraw-Hill, New York.

Donato, M. M. (2003), A statistical model for estimating stream temperatures in central Idaho, *Hydrol. Sci. Technol.*, *19*, 203–219.

Erickson, T. R., and H. G. Stefan (2000), Linear air/water temperature correlations for streams during open water periods, *J. Hydrol. Eng.*, *5*, 317–321, doi:10.1061/(ASCE)1084-0699(2000)5:3(317).

Goudsmit, G. H., H. Burchard, F. Peeters, and A. Wüest (2002), Application of the k-ε turbulence models to enclosed basins: The role of internal seiches, *J. Geophys. Res.*, *107*(12), 3230, doi:10.1029/2001JC000954.

Global Runoff Data Centre (GRDC) (2011), Long-Term Mean Monthly Discharges and Annual Characteristics of GRDC Station/Global Runoff Data Centre, Fed. Inst. of Hydrol. (BfG), Koblenz, Germany. [Available at http://www.bafg.de/cln_033/nn_294838/GRDC/ EN/02__Services/02__DataProducts/LongTermMonthlyMeans/longtermmonthly__node.html?__nnn =true; accessed 21/08/2012.]

Hicks, F., W. Cui, and D. Andres (1997), Modelling the thermal break up on the Mackenzie River at the outlet of Great Slave Lake, N.W.T., *Can. J. Civ. Eng.*, *24*, 570–585, doi:10.1139/l97-007.

Hodges, B. R., J. Imberger, A. Saggio, and K. B. Winters (2000), Modelling basin-scale internal waves in a stratified lake, *Limnol. Oceanogr.*, *45*(7), 1603–1620, doi:10.4319/lo.2000.45.7.1603.

Holdridge, L. R. (1967), *Life Zone Ecology*, Trop. Sci. Cent., San Jose, Costa Rica.

Hondzo, M., and H. G. Stefan (1994), Riverbed heat conduction prediction, *Water Resour. Res.*, *30*, 1503–1513, doi:10.1029/93WR03508.

Kim, K. S., and S. C. Chapra (1997), Temperature model for highly transient shallow streams, *J. Hydraul. Eng.*, *123*, 30–40, doi:10.1061/(ASCE)0733-9429(1997)123:1(30).

Kinzer, G. D., and R. Gunn (1951), Evaporation, temperature and thermal relaxation-time of freely falling waterdrops, *J. Meteorol.*, *8*, 71–83, doi:10.1175/1520-0469(1951)008<0071:TETATR>2.0.CO;2.

Leemans, R. (1989), Global Holdridge Life Zone Classifications, digital raster data on a 0.5-degree geographic (lat/long) 360 × 720 grid, http://www.ngdc.noaa.gov/ecosys/cdroms/ged_iia/datasets/a06/lh.htm#top, Natl. Geophys. Data Cent., Boulder, Colo.

Lehner, B., and P. Döll (2004), Development and validation of a global database of lakes, reservoirs and wetlands, *J. Hydrol.*, *296*, 1–22, doi:10.1016/j.jhydrol.2004.03.028.

Lighthill, M. J., and G. B. Whitham (1955), On kinematic waves. I. Flood movement in long rivers, *Proc. R. Soc. London, Ser. A*, *229*, 281–316, doi:10.1098/rspa.1955.0088.

Mironov, D. (2008), Parameterization of lakes in numerical weather prediction. Part 1: Description of a lake model, *COSMO Tech. Rep. 11*, Dtsch. Wetterdienst, Offenbach am Main, Germany.

Neumann, D. W., B. Rajagopalan, and E. A. Zagona (2003), Regression model for daily maximum stream temperature, *J. Environ. Eng.*, *129*, 667–674, doi:10.1061/(ASCE)0733-9372(2003)129:7(667).

New, M., M. Hulme, and P. D. Jones (1999), Representing twentieth century space-time climate variability. Part 1: Development of a 1961–90 mean monthly terrestrial climatology, *J. Clim.*, *12*, 829–856, doi:10.1175/1520-0442(1999)012<0829:RTCSTC>2.0.CO;2.

New, M., M. Hulme, and P. D. Jones (2000), Representing twentieth century space-time climate variability. Part 2: Development of 1901–96 monthly grids of terrestrial surface climate, *J. Clim.*, *13*, 2217–2238, doi:10.1175/1520-0442(2000)013<2217:RTCSTC>2.0.CO;2.

Nezhikovskiy, R. A. (1964), Coefficient of roughness of bottom surfaces of slush ice cover, *Sov. Hydrol. Sel. Pap.*, *2*, 127–150.

Perroud, M., S. Goyette, A. Martynov, M. Beniston, and O. Anneville (2009), Simulation of multiannual thermal profiles in deep Lake Geneva: A comparison of one-dimensional lake models, *Limnol. Oceanogr.*, *54*(5), 1574–1594, doi:10.4319/lo.2009.54.5.1574.

Rounds, S. A., T. M. Wood, and D. D. Lynch (1999), Modeling discharge, temperature and water quality in the Tualatin River, Oregon, *U.S. Geol. Surv. Water Supply Pap.*, *2465-B*.

Sinokrot, B. A., and H. G. Stefan (1993), Stream temperature dynamics: Measurements and modelling, *Water Resour. Res.*, *29*, 2299–2312, doi:10.1029/93WR00540.

Uppala, S. M., et al. (2005), The ERA-40 re-analysis, *Q. J. R. Meteorol. Soc.*, *131*, 2961–3012, doi:10.1256/qj.04.176.

U.S. Army Corps of Engineers (2002), Hydraulic computations and modeling of ice-covered rivers, engineering and design, in *Ice Engineering, Eng. Man. 1110–2-1612*, pp. 4.1–4.14, Washington, D. C.

van Beek, L. P. H., and M. F. P. Bierkens (2009), The global hydrological model PCR-GLOBWB: Conceptualization, parameterization and verification, report, Dep. of Phys. Geogr., Utrecht Univ., Utrecht, Netherlands [Available at http://vanbeek.geo.uu.nl/suppinfo/vanbeekbierkens2009.pdf.]

van Beek, L. P. H., Y. Wada, and M. F. P. Bierkens (2011), Global monthly water stress: 1. Water balance and water availability, *Water Resour. Res.*, *47*, W07517, doi:10.1029/2010WR009791.

van Vliet, M. T. H., F. Ludwig, J. J. G. Zwolsman, G. P. Weedon, and P. Kabat (2011), Global river temperatures and the sensitivity to atmospheric warming and changes in river flow, *Water Resour. Res.*, *47*, W02544, doi:10.1029/2010WR009198.

Verdin, K. L., and S. K. Greenlee (1996), Development of continental scale digital elevation models and extraction of hydrographic features, paper

presented at 3rd International Conference/Workshop on Integrating GIS and Environmental Modeling, Natl. Cent. for Geogr. Inf. and Anal., Santa Barbara, Calif.

Vörösmarty, C. J., et al. (2010), Global threats to human water security and river biodiversity, *Nature*, *467*, 555–561, doi:10.1038/nature09440.

Wang, P. F., and J. L. Martin (1991), Temperature and conductivity modelling for the Buffalo River, *J. Great Lakes Res.*, *17*, 495–503, doi:10.1016/S0380-1330(91)71385-3.

Webb, B. W. (1996), Trends in stream and river temperature, *Hydrol. Processes*, *10*, 205–226, doi:10.1002/(SICI)1099-1085(199602)10:2<205::AID-HYP358>3.0.CO;2-1.

Webb, B. W., D. M. Hannah, R. D. Moore, L. E. Brown, and F. Nobilis (2008), Recent advances in stream and river temperature research, *Hydrol. Processes*, *22*, 902–918, doi:10.1002/hyp.6994.

Younus, M., M. Hondzo, and B. A. Engel (2000), Stream temperature dynamics in upland agricultural watersheds, *J. Environ. Eng.*, *126*, 518–526, doi:10.1061/(ASCE)0733-9372(2000)126:6(518).